

We are IntechOpen, the world's leading publisher of Open Access books Built by scientists, for scientists

6,900

Open access books available

186,000

International authors and editors

200M

Downloads

Our authors are among the

154

Countries delivered to

TOP 1%

most cited scientists

12.2%

Contributors from top 500 universities



WEB OF SCIENCE™

Selection of our books indexed in the Book Citation Index
in Web of Science™ Core Collection (BKCI)

Interested in publishing with us?
Contact book.department@intechopen.com

Numbers displayed above are based on latest data collected.
For more information visit www.intechopen.com



The Sources Reconstruction Method for Antenna Diagnostics and Imaging Applications

Yuri Álvarez, Fernando Las-Heras and
Cebrián García

Additional information is available at the end of the chapter

<http://dx.doi.org/10.5772/50744>

1. Introduction

The advances on communications systems require more challenging antenna designs, increasing the complexity of design, manufacturing, and testing stages. Different sources of error may affect the antenna final prototype, degrading its performance, and then requiring a re-design step to identify and correct these manufacturing errors. In general, this re-design step requires invasive techniques based on trial-error procedure, whose technical and economical costs are directly related to the antenna complexity. For this reason, the development of fast and accurate non-invasive methods for antenna faults detection (antenna diagnostics) has been of great interest in the last decade.

This chapter describes the Sources Reconstruction Method (SRM), an integral equation-based inverse technique, and its applications on antenna diagnostics, near-field to far-field transformation, and the recent advances on imaging applications. The method provides an electromagnetic model of the problem-under-study based on an equivalent currents distribution, which can be used to evaluate the field radiated at any point of the space. The equivalent model can be used for antenna diagnostics applications in the field of antenna measurements, as well as for geometry reconstruction purposes in the case of scattering acquisitions.

1.1. Antenna Diagnostics

Antenna diagnostics comprises these techniques based on the recovery of the extreme near-field of the Antenna-Under-Test (AUT) from the field radiated by it. Extreme near-field is defined as the field in the proximity of the AUT (i.e. a distance < 1 wavelength (λ), or on the AUT aperture plane). The field radiated by the AUT can be acquired in the near or far field region (Yaghian, 1986).

The extreme near-field is strongly related to the physical currents (in the case of metallic surfaces) or aperture field distribution of the AUT. In consequence, an accurate retrieval of this field provides a useful mapping of the fields and currents distribution on the manufactured antenna, which can be compared to the initial design to identify which parts of the antenna have faults or differences with respect to the designed one.

1.1.1. Backpropagation techniques

It is well-known that the AUT radiation pattern can be calculated as the Fourier Transform of the fields on the AUT aperture plane (Yaghian, 1986). In consequence, this calculation can be reverted in order to recover the AUT aperture fields from the radiation pattern. The simplest case relates a planar field acquisition domain with the AUT aperture plane. For example, in (Kaplan et al., 1979; Rahmat-Samii, 1984) the fields acquired on a plane are backpropagated to the aperture plane by using the inverse Fast Fourier transform (iFFT). Polar and bi-polar measurement setups are also suitable for this kind of technique (Gatti & Rahmat-Samii, 1988; Yaccarino et al., 1994), which has been extended to phaseless measurements (Yaccarino & Rahmat-Samii, 1999; Razavi & Rahmat-Samii, 2007). Equivalent current techniques have been also developed (Petre & Sarkar, 1992), showing similar performance to the iFFT-based methods.

Next step was the aperture field calculation from the field acquired in spherical domains, which is one of the most extended antenna measurement systems (Yaghian, 1986). A formulation relating spherical wave modes with the AUT plane wave spectrum has been developed in (Cappellin et al., 2008). Also equivalent current methods have been extended to this measurement setup, providing the same accuracy as wave mode based techniques (Álvarez et al., 2008c).

It is out of doubt that fastest diagnostics results are given by iFFT-based methods. So for many years, the computational cost of equivalent current techniques, derived from a kind of inverse Method-of-Moments (MoM), was prohibitive for practical antenna diagnostics. However, the increase of antenna design complexity requires the extreme near-field to be recovered not only in the AUT aperture plane, but also in a surface fitting the AUT geometry. The need of this requirement, together with the improvement of calculation resources fostered the development of equivalent current techniques.

1.1.2. Three-dimensional techniques

Wave mode-based techniques are limited to canonical geometries (mainly planar, cylindrical, and spherical), for both reconstruction domain (e.g. extreme near-field) and field acquisition domain. Equivalent current methods for antenna diagnostics are able to overcome this limitation, so that arbitrary geometry domains can be defined. The only limitation is that the extreme near-field surface must enclose all the radiating elements.

Equivalent current methods provide an accurate electromagnetic model of the AUT, that has been mainly used for antenna diagnostics, as for example, detection of faulting elements in antenna arrays (Álvarez et al., 2009b), reflector antenna distortions (Álvarez et al., 2008c; Las-

Heras et al., 2009), leakage identification (Foged et al., 2011a), and parasitic currents in antenna elements (Araque & Vecchi, 2009). In addition to the equivalent current techniques, it has been proposed the use of electric and magnetic infinitesimal dipoles that model the AUT electromagnetic behaviour (Sijher & Kishk, 2005; Mikki & Kishk, 2007). The orientation and excitation of these infinitesimal dipoles is determined from the acquired near-field distribution.

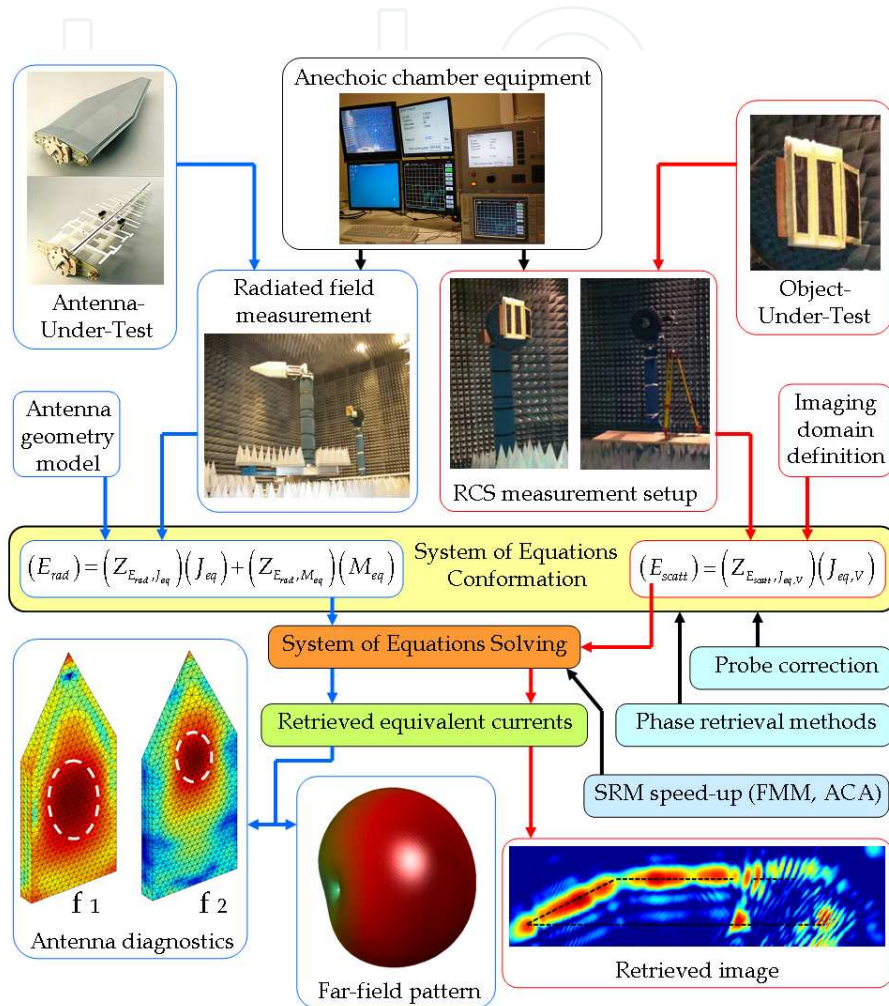


Figure 1. General scheme showing the equivalent current (or sources reconstruction) method for antenna diagnostics and geometry reconstruction.

Apart from antenna diagnostics, these techniques have potential applications in other antenna measurement related topics: near-field to far-field transformation (that is, antenna radiation pattern calculation) (Las-Heras et al., 2006; Álvarez et al., 2008a; Álvarez et al., 2007; Álvarez et al., 2012b), analysis of the AUT interaction with scatterers (Las-Heras, 2001; García et al., 2011), filtering of parasitic elements (Araque & Vecchi, 2009; Cano et al., 2010) and electromagnetic emissions analysis (Laviada et al., 2010; Hernando et al., 2008; Persson & Gustafsson, 2005; Eibert & Schmidt, 2009). Due to its wide field of applications, some antenna measurement companies have even released their own antenna diagnostics software, as for example (Foged et al., 2011b) and (Cappellin et al., 2011).

Equivalent current methods have been extended to cope with phaseless measurements (Las-Heras & Sarkar, 2002; Álvarez et al., 2010c; Álvarez et al., 2012b) which are of special interest on sub-mm and THz frequency bands, where phase measurements require expensive equipment (Hellicar et al., 2009; Hislop & Hellicar, 2009).

1.2. Inverse scattering methods based on equivalent Currents

Equivalent currents provide an equivalent model of the AUT that can be also extrapolated to scattering problems. In this case, the scatterer is illuminated by an incident field, inducing a set of currents on the object. Thus, if the incident and scattered fields are known, it would be possible to recover an equivalent currents distribution related to the scatterer geometry. For metallic objects the idea is simple: the equivalent currents intensity will be related to the regions of the space where the physical induced currents are flowing.

Several inverse scattering techniques are based upon this idea (Habashy et al., 1990; Caorsi et al., 1990; Qin & Ciric, 1993; Van den Berg, Kleimann, 1997; Lin & Kiang, 1996; Álvarez et al., 2010b). The main limitation is the need of volumetric equivalent currents domains, which significantly increases the calculation time. Computational acceleration schemes can be applied to reduce it.

To sum up this section, general schemes of the equivalent current techniques, also referred as Sources Reconstruction Method (SRM), is presented in Fig. 1, together with its applications to antenna diagnostics and characterization, near-field to far-field transformation, and profile reconstruction.

2. The Sources Reconstruction Method

The concept of the Sources Reconstruction Method (SRM) is illustrated in Fig. 2. On the left, the direct radiation problem is plotted: the field radiated by the AUT (E_{rad}) is collected on the acquisition domain S_{obs} . Now, the SRM goal is to recover the extreme near-field on a surface S' enclosing the AUT. The field samples (E_{rad}) are *backpropagated* from S_{obs} to S' (Fig. 2, right) obtaining an electromagnetic equivalent currents distribution, $J_{\text{eq}}, M_{\text{eq}}$. These equivalent currents radiate the same electromagnetic fields as the AUT outside the domain enclosed by S' ; in other words, the currents provide an *equivalent* electromagnetic model of the AUT.

2.1. The electromagnetic equivalence principle

The SRM is based on the electromagnetic Equivalence Principle (Harrington, 2001; Stratton, 1941; Balanis, 1997): consider the fields (E_n, H_n) and currents (J_n, M_n) defined in Fig. 3 (a) where two media are present: an inner medium ($n=1$) with constitutive parameters $\epsilon_1, \mu_1, \sigma_1$, defined in the volume V' , and bounded by S' ; and the outer medium ($n=2$), with constitutive parameters $\epsilon_2, \mu_2, \sigma_2$.

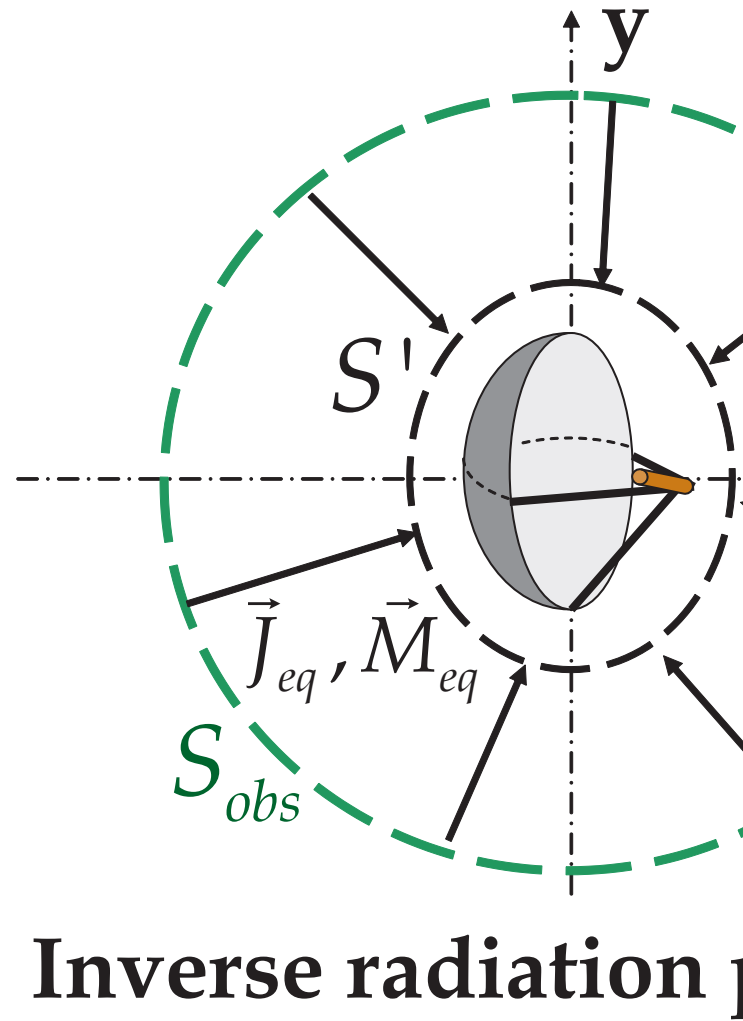
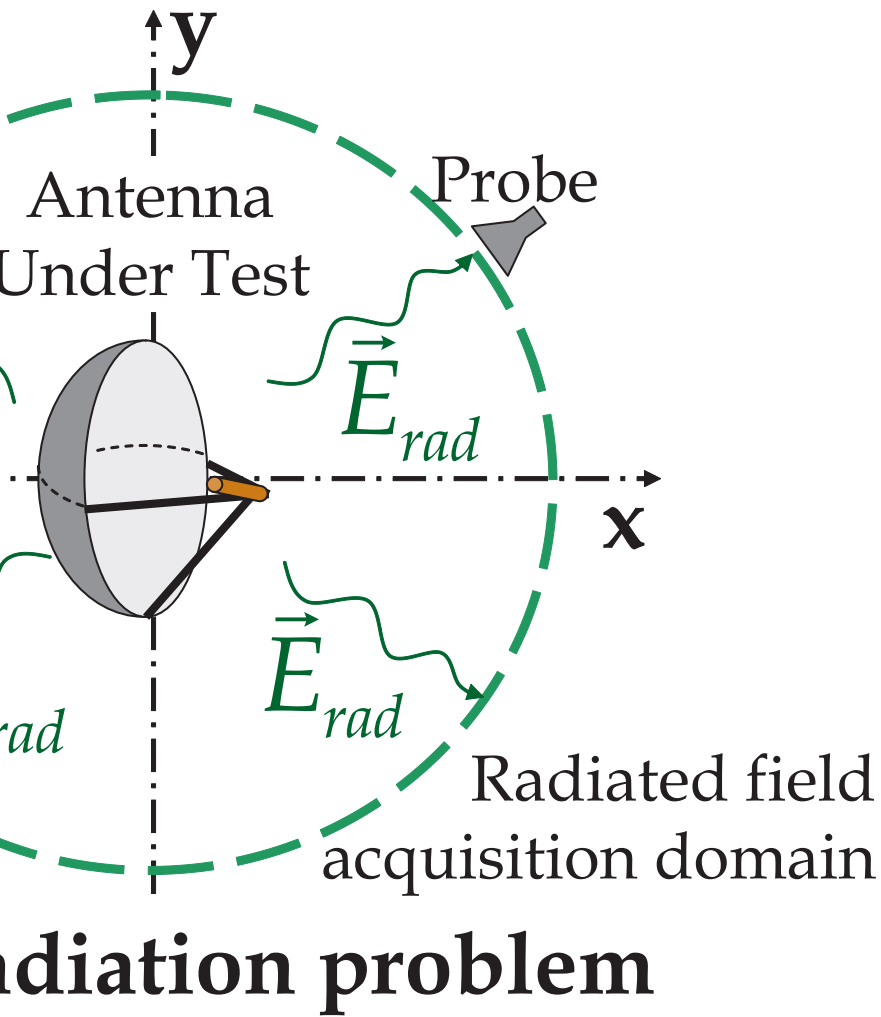


Figure 2. Direct and inverse radiation problem.

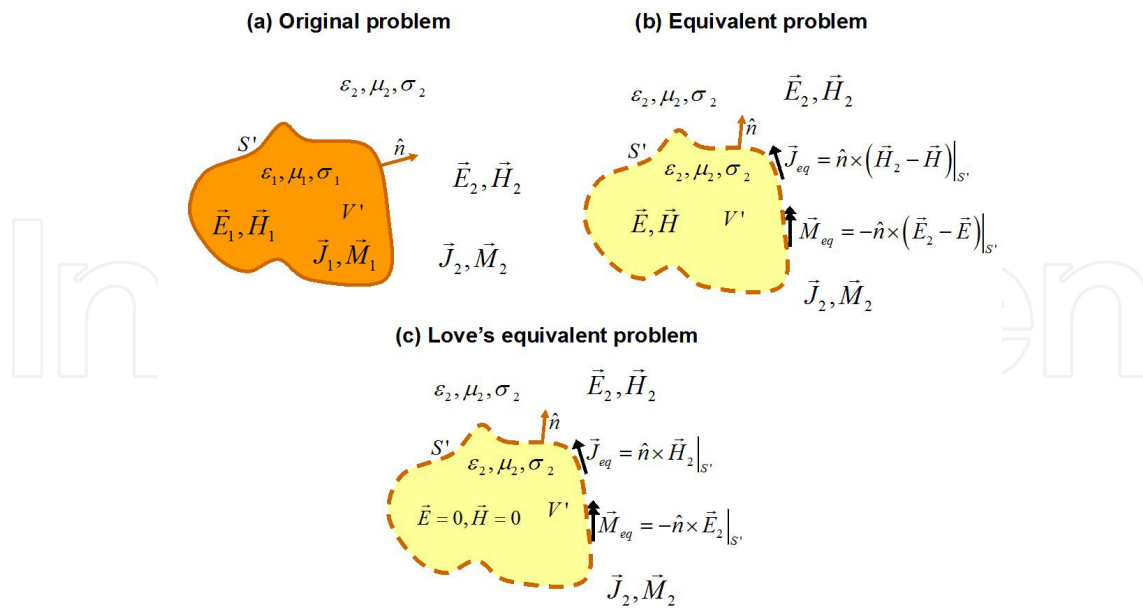


Figure 3. Electromagnetic Equivalence Principle.

In Fig. 3 (b), a set of equivalent electric (J_{eq}) and magnetic currents (M_{eq}) is defined on the boundary between the two media (S'). These currents are defined as the gap between the tangential components of the fields in media 1,2. Note that no assumption about the fields and currents inside S' is considered, just imposing the currents to radiate the same fields outside S' as in Fig. 3 (a). In consequence, J_{eq} and M_{eq} characterize the electromagnetic behaviour *outside* S' of the fields (E_1, H_1) and currents (J_1, M_1) enclosed by S' .

Several SRM implementations (Foged et al., 2011a; Araque & Vecchi, 2009; Cappellin et al., 2011; Araque & Vecchi, 2010) make use of the Love's Equivalence Principle: in this case, the fields inside S' are forced to be zero (Fig. 3 (c)), so that the equivalent currents on S' are directly the field tangential components. In the case of antenna diagnostics, they correspond to the extreme near-fields.

2.2. Integral Equations

The Sources Reconstruction Method (SRM) is based on the integral equations relating the electromagnetic field (E_{rad}) observed in S_{obs} with their sources. In the case of the SRM, the sources are the equivalent currents J_{eq} and M_{eq} defined on S' (Fig. 2 (b)).

The integral equations relating the electric field with an equivalent electric $J_{eq}(\mathbf{r}')$ and magnetic $M_{eq}(\mathbf{r}')$ currents distribution defined on a surface S' are given by Eqs. (1) and (2) respectively (Harrington, 2001; Balanis, 1997), so that the total electric field is the sum of the electric field due to electric currents $E_{rad,J_{eq}}(\mathbf{r})$ and the electric field due to magnetic currents $E_{rad,M_{eq}}(\mathbf{r})$.

$$\vec{E}_{rad, J_{eq}}(\vec{r}) = -\frac{j\eta_0}{4\pi k_0} \int_{S'} \left\{ k_0^2 \frac{e^{-jk_0 R(\vec{r}; \vec{r}')}}{R(\vec{r}; \vec{r}')} \vec{J}_{eq}(\vec{r}') + \nabla \left(\nabla \cdot \left(\frac{e^{-jk_0 R(\vec{r}; \vec{r}')}}{R(\vec{r}; \vec{r}')} \vec{J}_{eq}(\vec{r}') \right) \right) \right\} dS' \quad (1)$$

$$\vec{E}_{rad, M_{eq}}(\vec{r}) = -\frac{1}{4\pi} \int_{S'} \nabla \times \left(\frac{e^{-jk_0 R(\vec{r}; \vec{r}')}}{R(\vec{r}; \vec{r}')} \vec{M}_{eq}(\vec{r}') \right) dS' \quad (2)$$

where k_0 is the wavenumber, η_0 the intrinsic impedance, \vec{r} the position vector of the points where the field is acquired (surface S_{obs}), and \vec{r}' the position vector of the points where the currents are reconstructed, which belong to the S' domain. $R(\vec{r}; \vec{r}')$ is defined as $|\vec{r} - \vec{r}'|$.

2.3. Numerical solution

Integral equations (1), (2) have to be discretized for a numerical solution. The field observation domain (surface S_{obs}) is sampled in N points. The equivalent currents domain (S') is discretized in M planar facets (e.g. triangular facets or Rao-Wilton-Glisson basis functions (Rao et al., 1982) when modelling arbitrary 3D geometries).

Equivalent currents vectors are expressed as a linear combination of two perpendicular components defined on each facet $\Delta S'_m$. These components are referred to an orthogonal coordinate system defined on each facet using the unitary vectors $\hat{u}_m, \hat{v}_m, \hat{n}_m$ (see Fig. 4).

The definition of the components is given by Eq. (3), assuming that the equivalent currents are constant on each facet. This approach is, in general, valid, provided that $\Delta S'_m \ll (\lambda)^2$.

$$\begin{aligned} \vec{J}_{eq,m} &= J_{eq,u_m} \hat{u}_m + J_{eq,v_m} \hat{v}_m \\ \vec{M}_{eq,m} &= M_{eq,u_m} \hat{u}_m + M_{eq,v_m} \hat{v}_m \end{aligned} \quad (3)$$

The discretized integral equations as a function of indexes m, n , are described by (4), (5). All the constants and variables are known except the complex coefficients $J_{eq,um}, J_{eq,vm}, M_{eq,um}, M_{eq,vm}$.

$$\vec{E}_{rad, J_{eq}}(\vec{r}_n) = -\frac{j\eta_0}{4\pi k_0} \sum_{m=1}^M \left\{ \left(k_0^2 \frac{e^{-jk_0 R(\vec{r}_n; \vec{r}_m')}}{R(\vec{r}_n; \vec{r}_m')} + \nabla \left(\nabla \cdot \left(\frac{e^{-jk_0 R(\vec{r}_n; \vec{r}_m')}}{R(\vec{r}_n; \vec{r}_m')} \right) \right) \right) \cdot \left(J_{eq,u_m} \hat{u}_m + J_{eq,v_m} \hat{v}_m \right) \Delta S'_m \right\} \quad (4)$$

$$\vec{E}_{rad, M_{eq}}(\vec{r}_n) = -\frac{1}{4\pi} \sum_{m=1}^M \left\{ \nabla \times \left(\frac{e^{-jk_0 R(\vec{r}_n; \vec{r}_m')}}{R(\vec{r}_n; \vec{r}_m')} \left(M_{eq,u_m} \hat{u}_m + M_{eq,v_m} \hat{v}_m \right) \right) \Delta S'_m \right\} \quad (5)$$

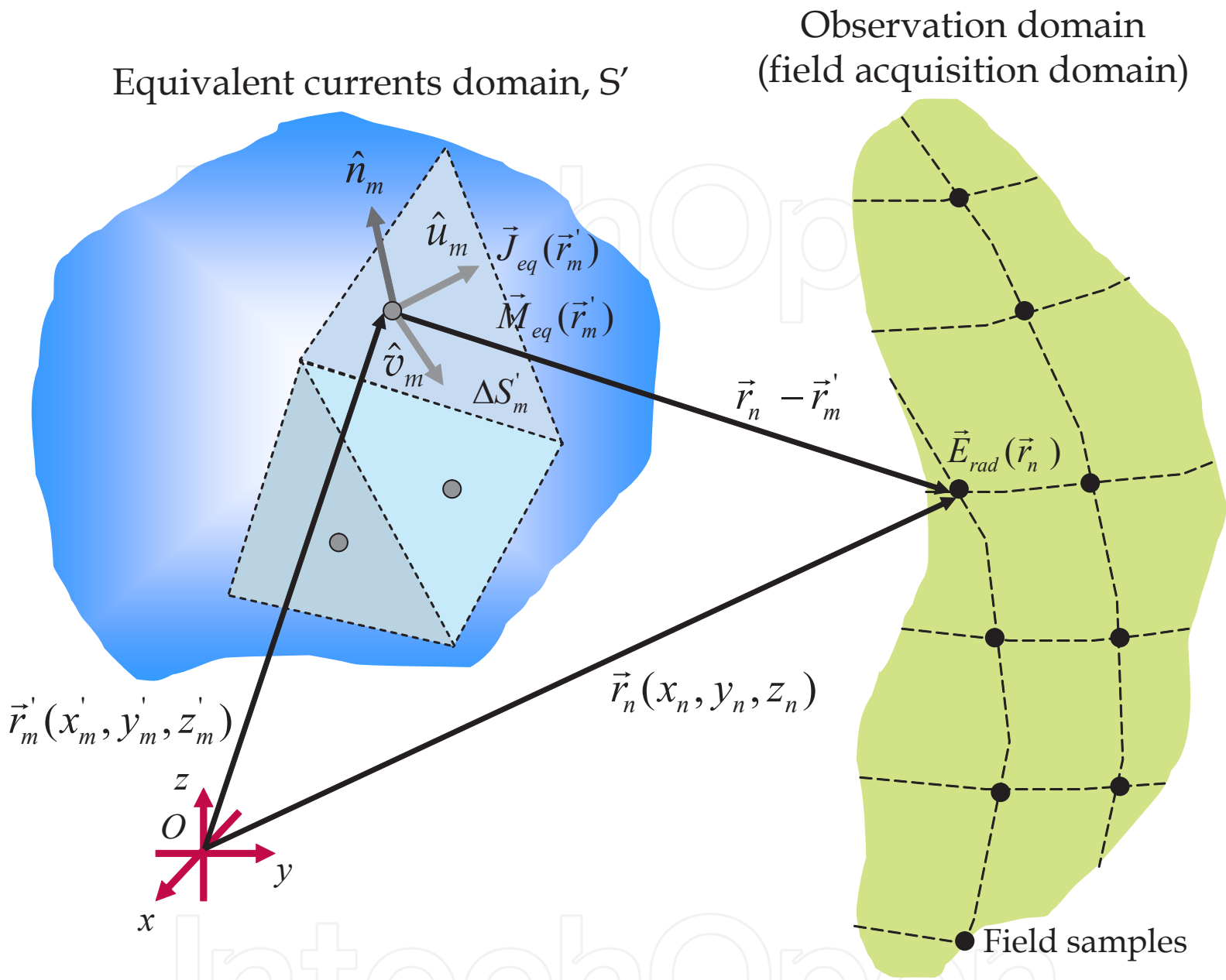


Figure 4. Definition of the observation and equivalent currents domain, and how they are discretized.

The discretized equations can be rewritten in a more compact form, resulting in the matrix system (6). The unknown coefficients of the equivalent currents correspond to the right column vector of (6), the field samples correspond to the independent column vector, and the rest of variables and coefficients of Eqs. (4) and (5) are grouped in a matrix called Z-matrix.

$$\begin{pmatrix} E_{rad}^{t_1} \\ E_{rad}^{t_2} \end{pmatrix} = \begin{pmatrix} Z_{E_{rad}^{t_1}; J_{eq,u}} & Z_{E_{rad}^{t_1}; J_{eq,v}} & Z_{E_{rad}^{t_1}; M_{eq,u}} & Z_{E_{rad}^{t_1}; M_{eq,v}} \\ Z_{E_{rad}^{t_2}; J_{eq,u}} & Z_{E_{rad}^{t_2}; J_{eq,v}} & Z_{E_{rad}^{t_2}; M_{eq,u}} & Z_{E_{rad}^{t_2}; M_{eq,v}} \end{pmatrix} \begin{pmatrix} J_{eq,u} \\ J_{eq,v} \\ M_{eq,u} \\ M_{eq,v} \end{pmatrix} \quad (6)$$

The field samples on S_{obs} can be expressed by means of 3 orthogonal components: $E_{rad} = E_{rad,t1} \mathbf{t}_1 + E_{rad,t2} \mathbf{t}_2 + E_{rad,n} \mathbf{n}$. The majority of antenna measurement systems only acquire the tangential field components, as the normal component decay much faster than the tangential ones. Thus, only the tangential field components ($E_{rad,t1}, E_{rad,t2}$) are used to recover the equivalent currents. These tangential components can be referred to the corresponding canonical coordinate systems. For example, in the case of cylindrical acquisition system, $\mathbf{t}_1 = \phi$, $\mathbf{t}_2 = z$. In spherical system: $\mathbf{t}_1 = \theta$, $\mathbf{t}_2 = \varphi$.

The resulting linear system of equations has $2 \times N$ equations and $4 \times M$ unknowns. Sometimes, it is possible to use just one type of equivalent currents if the reconstruction domain S' is a flat surface (Petre & Sarkar, 1992; Las-Heras et al., 2006; Sarkar & Taaghoul, 1999). In this case, the observation domain is restricted to one of the two halves of the space divided by the virtual infinite plane containing S' .

2.4. Numerical solvers

Different techniques can be used to solve the linear system of equations (6). In general, the number of equations (N_e) and unknowns (M_u) may be different; $N_e \neq M_u$ i.e. the system of equations may not be square. In addition, depending on the Z-matrix rank and the number of unknowns, the system can be overdetermined ($Rank(Z\text{-matrix}) > M_u$) or undetermined ($Rank(Z\text{-matrix}) < M_u$). The numerical solvers considered in this section seek for the least mean squares solution, that is, the equivalent currents distribution that minimizes the error (ϵ) between the acquired field samples and the field radiated by the reconstructed equivalent currents evaluated on the field sampling points. The issue of the solution accuracy is also discussed in detail in (Araque & Vecchi, 2010), analyzing the system conditioning and discussing several regularization techniques.

Table 1 summarizes the solvers that have been tested. Regarding computational cost considerations, $N \approx M \approx N_e \approx M_u$ is assumed¹.

Singular Value Decomposition (SVD) calculates the singular values of the Z-matrix (Álvarez et al., 2009b; Araque & Vecchi, 2010), providing a valuable analysis about its conditioning: if the problem is ill-conditioned (high condition number) (Sarkar et al., 1981b), that means that the solution of the problem (equivalent currents) is quite sensitive to small changes in the inputs (i.e. the field samples). Lower singular values can be neglected (Truncated-SVD) (Álvarez et al., 2009b; Araque & Vecchi, 2010), improving the Z-matrix conditioning, and then

¹ Notation: N denotes the number of field samples, and N_e the number of equations. M defines the number of equivalent currents facets, and M_u the number of unknowns.

stabilizing the solution. The main drawback of this technique is the moderate computational cost ($O(N^3)$) as the SVD requires the calculation of the pseudoinverse of the Z-matrix.

Method	Type	Time $O(N)$	Memory $O(N)$
Singular Value Decomposition (SVD)	Matrix inversion	$O(N^3)$	$O(N^2)$
Conjugate Gradient (GC)	Iterative	$O(N^2)$	$O(N^2)$
Memory Saving Technique (MST) ⁽¹⁾	Iterative ⁽¹⁾	$O(N^2)$	$O(N)$
Fast Multipole Method (FMM) ⁽¹⁾	Iterative ⁽¹⁾	$O(N^{1.5})$	$O(N^{1.5})$
Adaptive Cross Approximation algorithm (ACA) ⁽¹⁾	Iterative ⁽¹⁾	$O(N^{4/3} \log N)$	$O(N^{4/3} \log N)$

⁽¹⁾ These techniques are implemented over the CG method.

Table 1. Numerical techniques and computational cost.

A more affordable implementation in terms of calculation time relies on iterative solvers. Among different techniques, the Conjugate Gradient (CG) (Sarkar & Arvas, 1981a) has been found to provide a good trade-off between calculation time $O(N^2)$ and accuracy, and in particular, the implemented CG algorithm (Wang & Hwang, 1995) has a monotonically decrease of the error (ϵ). Iterative solvers require the definition of stopping rules or criteria. In this case, the first rule is the definition of a maximum number of iterations, K . The second rule is the variation of the error ($\Delta\epsilon$) between two consecutive iterations: $\Delta\epsilon(k) = \epsilon(k-1) - \epsilon(k)$. If this variation is smaller than a fixed threshold, the CG finishes. Typical threshold values can be $\Delta\epsilon = 0.001 - 0.01$ (Álvarez et al., 2009b; López et al., 2012). In order to provide a reference, convergence is usually reached in no more than $K = 20$ iterations with $\epsilon < 0.05$ for the given $\Delta\epsilon$ threshold values in practical antenna measurements.

Electrically large antenna diagnostics may require a significant amount of calculation time. To reduce it, different computational acceleration schemes have been applied over the CG formulation. The first one was the Fast Multipole Method (FMM) (Eibert & Schmidt, 2009; Engheta et al., 1992; Coifman et al., 1993): in brief, the idea is to approximate field and source samples which belong to a certain region in terms of plane and spherical waves. In general, FMM is applied to problems in which all the regions belong to the same physical domain, so interactions between adjacent regions have to be analyzed without the FMM approach. In the case of the SRM, the source (equivalent currents) and field samples belong to different physical domains (Fig. 2) (Eibert & Schmidt, 2009; Álvarez et al., 2008b), avoiding the presence of adjacent regions.

Another tested acceleration technique was the Adaptive Cross Approximation (ACA) algorithm. While the FMM takes advantage of the physical properties of the problem (i.e. the fields and currents approach in terms of plane and spherical waves), the ACA exploits the algebraic properties of the Z-matrix (Álvarez et al., 2009a). Assuming that the Z-matrix is rank deficient, then, it can be approximated as Z-matrix = $U \times V$. Considering that the Z-

matrix has N_e rows and M_u columns, then U has N_e rows and R columns, and V , R rows and M_u columns, where R is defined as the effective rank of the Z -matrix (Zhao et al., 2005). ACA is an efficient acceleration technique both in time and memory provided that $(N_e + M_u) R \ll N_e \times M_u$ (Zhao et al., 2005; Álvarez et al., 2009a).

Finally, the inner CG implementation allows a quite efficient memory saving technique at the expense of increasing the calculation time. This method relies on the fact that the Z -matrix elements can be calculated using mathematical expressions (4), (5) if the indexes m, n are known. In consequence, instead of calculating and storing the entire Z -matrix, the Z -matrix elements are calculated every time they are needed, reducing the memory consumption from $O(N^2)$ to $O(N)$. As an example, consider a problem with similar number of field samples and facets, $N_e \sim M_u \sim 100,000$. The Z -matrix storage would require 150 GB of memory. The memory saving technique requires less than 100 MB of memory (Álvarez et al., 2007; López et al., 2012).

Graphics Processing Units (GPU) is the ultimate technology for hardware acceleration in those problems demanding intensive calculations. The above mentioned memory saving technique fulfils these requirements for GPU implementation, providing a speed-up greater than 70 times with respect to previous CPU implementation (Álvarez et al., 2009b; Álvarez et al., 2007). As an example, an antenna diagnostics problem with $\sim 20,000$ field samples and $\sim 20,000$ equivalent currents facets is solved in just 30 s (López et al., 2012).

2.5. Extension to inverse scattering problems

2.5.1. Inverse scattering methods for geometry reconstruction

The SRM extension to inverse scattering problems can be classified as an inverse source problem technique (Habashy et al., 1990; Caorsi et al., 1990; Qin & Ciric, 1993; Van den Berg, Kleimann, 1997; Álvarez et al., 2010b), that pursues the geometry and constitutive parameters estimation by retrieving a set of equivalent sources. While the geometry reconstruction problem yields a linear system of equations, constitutive parameters retrieval involves a non-linear system of equations, increasing the inverse problem complexity.

Focusing on the geometry reconstruction case, other techniques have been developed. One is the Linear Sampling Method (Colton et al., 2003), which determines if a point on the region of interest belongs to the object-under-test or not. Its interest lies on its simplicity, as just a linear system of equations has to be solved.

Other methods are based on contour parameterization: starting from an initial guess, the parameterized geometry is modified until one that satisfies an imposed boundary condition (e.g. zero tangential field in case of perfect electric conductors (PEC) or tangential field continuity on dielectric surfaces) is found. The resulting system of equations relating the contour coordinates and the scattered field is non-linear, and it is necessary to use non-linear optimization methods to solve it (Lin & Kiang, 1996; Farmahini, 2009; Martínez et al., 2011; Hajihashemi & El-Shenawee, 2011). As the entire contour is optimized at the same time, these inversion methods usually require a remarkable amount of calculation time. Addition-

ally, as the cost function to be optimized is non-linear, the inversion process can easily get trapped in local minima.

2.5.2. The Volumetric SRM

As indicated before, the analysis of the extreme near-field provides information about the physical currents flowing on the metallic structure of the antenna. For example, consider the case depicted in Fig. 5: the equivalent currents recovered on the radome enclosing the Yagi-Uda antenna elements provide information about their position inside the radome.

Taking into account this fact, it has been considered the possibility of extending the SRM for inverse scattering problems (Volumetric SRM) (Álvarez et al., 2010b); in particular, for metallic objects geometry reconstruction. The idea is to retrieve the electric currents induced by an incident field. As in the case of the Yagi-Uda antenna in Fig. 5, it is expected that the highest intensity of the reconstructed equivalent currents will be related to the placement of the physical induced currents.

The direct and inverse scattering problem using equivalent currents are depicted in Fig. 6. The main difference with respect to the SRM for antenna diagnostics is the use of a volumetric equivalent currents distribution ($J_{eq,V}$): now, the reconstruction domain is a volume V' enclosing the metallic scatterers, so the field radiated by the reconstructed equivalent currents $J_{eq,V}$ is the same as the field scattered by the original geometry (Volumetric Equivalence Principle (Livesay & Chen, 1974)). The integral equation relating the scattered field (E_{scatt}) with the volumetric equivalent currents ($J_{eq,V}$) is (7) (Álvarez et al., 2010a; Álvarez et al., 2010b).

$$\vec{E}_{scatt}(\vec{r}) = -\frac{j\eta_0}{4\pi k_0} \int_{V'} \left\{ k_0^2 \frac{e^{-jk_0 R(\vec{r};\vec{r}')}}{R(\vec{r};\vec{r}')} \vec{J}_{eq,V}(\vec{r}') + \nabla \left(\nabla \cdot \left(\frac{e^{-jk_0 R(\vec{r};\vec{r}')}}{R(\vec{r};\vec{r}')} \vec{J}_{eq,V}(\vec{r}') \right) \right) \right\} dV' \quad (7)$$

One of the main drawbacks of the Volumetric SRM is the problem dimensionality, which is increased from $O(N^2)$ to $O(N^3)$. For electrically large scatterers, the domain V' may be too large to be analyzed in a reasonable time even with a powerful workstation. To overcome this drawback, an inverse Fast Multipole Method (iFMM) has been developed in (Álvarez et al., 2011) (2D) and (Álvarez et al., 2012a) (3D) allowing a significant speed-up (up to 500 times) without compromising the accuracy of the retrieved geometry. Even more, the use of a Dyadic formulation (7) provides an advantage with respect to scalar formulations (López-Sánchez & Fortuny-Guash, 2000) as polarization information can be efficiently used to improve the quality of the reconstruction.

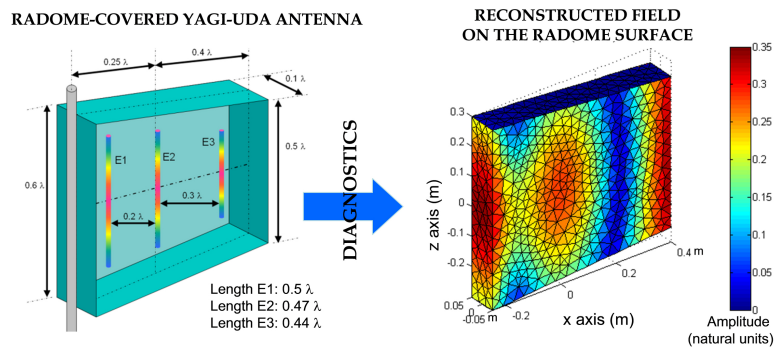
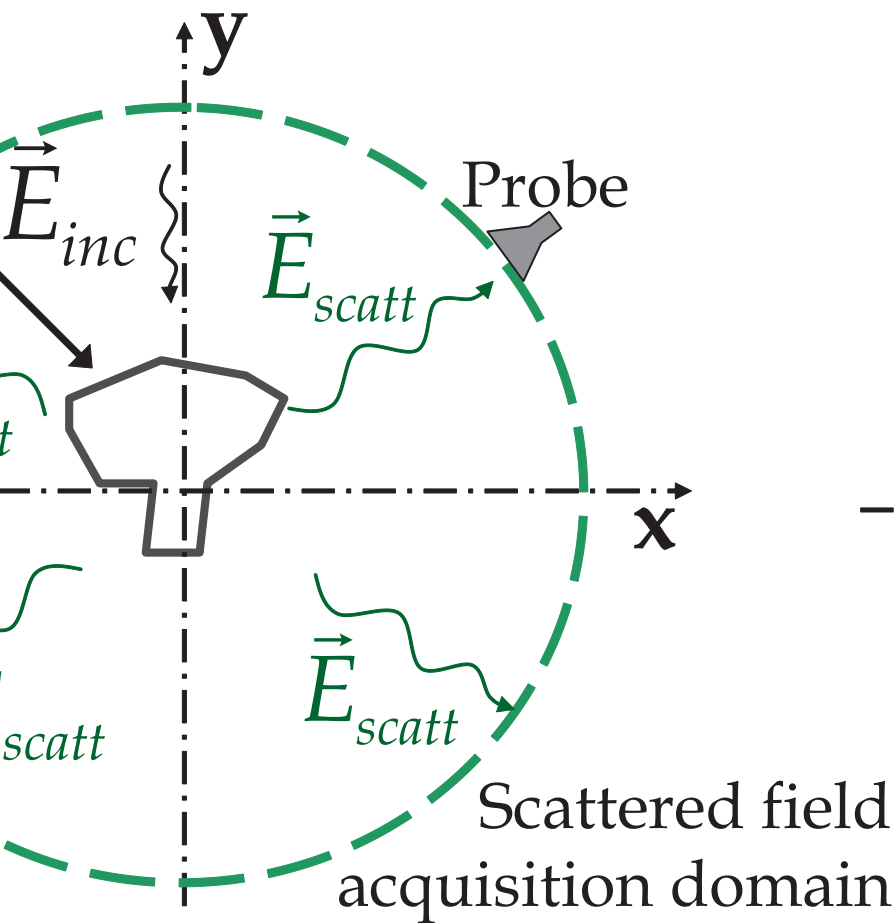
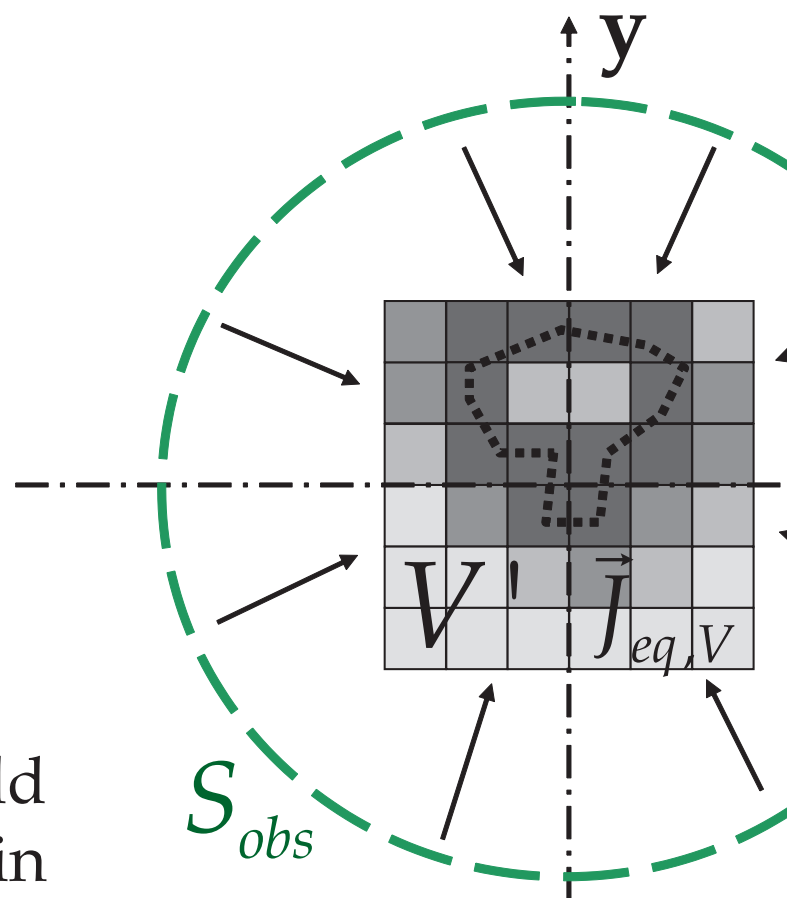


Figure 5. Antenna diagnostics of a 3-element Yagi-Uda antenna covered by a radome.



scattering problem



Inverse scattering

Figure 6. Direct and inverse scattering problems using equivalent currents.

3. Application examples

3.1. Antenna array diagnostics

The first application example is devoted to clearly show the antenna diagnostics capabilities of the SRM. For this purpose, a 3x3 antenna array of $\lambda/2$ dipoles has been designed and simulated. Nominal excitations are plotted in Fig. 7. In order to simulate a failure in two antenna array elements, dipoles 2 and 4 are distorted, reducing their feeding from 0 dB to -6 dB and -30 dB respectively. A Method-of-Moments code is used to analyze the antenna and to evaluate the radiation pattern, which is depicted in Fig. 7: it is clear that the distortion introduced in a two elements array antenna degrades the radiation pattern, but no information about the malfunctioning elements can be extracted from the pattern.

The SRM is applied to retrieve an equivalent currents distribution on the antenna array aperture plane. The reconstructed equivalent currents will be related to the extreme near-field and hence, to the nominal excitations of the antenna, so any failure in the array elements can be identified.

The working frequency is $f = 300$ MHz. The antenna size is defined in terms of the minimum sphere enclosing the array (R_{\min}), which is $R_{\min} = \sim 1.5$ m, so according to (Hansen, 1988; Yahghian, 1986) the minimum number of radiation pattern samples for this antenna is $N=441$: $\theta = [-90^\circ + 90^\circ]$, with $\Delta\theta = 9^\circ$, and $\varphi = [0^\circ 180^\circ]$, with $\Delta\varphi = 9^\circ$. The equivalent currents are reconstructed in a planar domain $S' = (3 \times 3 \text{ m})^2$, discretized in $M = 441$ facets ($\Delta S' = (0.15 \times 0.15 \text{ m})^2$) in order to have, for this particular case, the same number of field samples and equivalent currents.

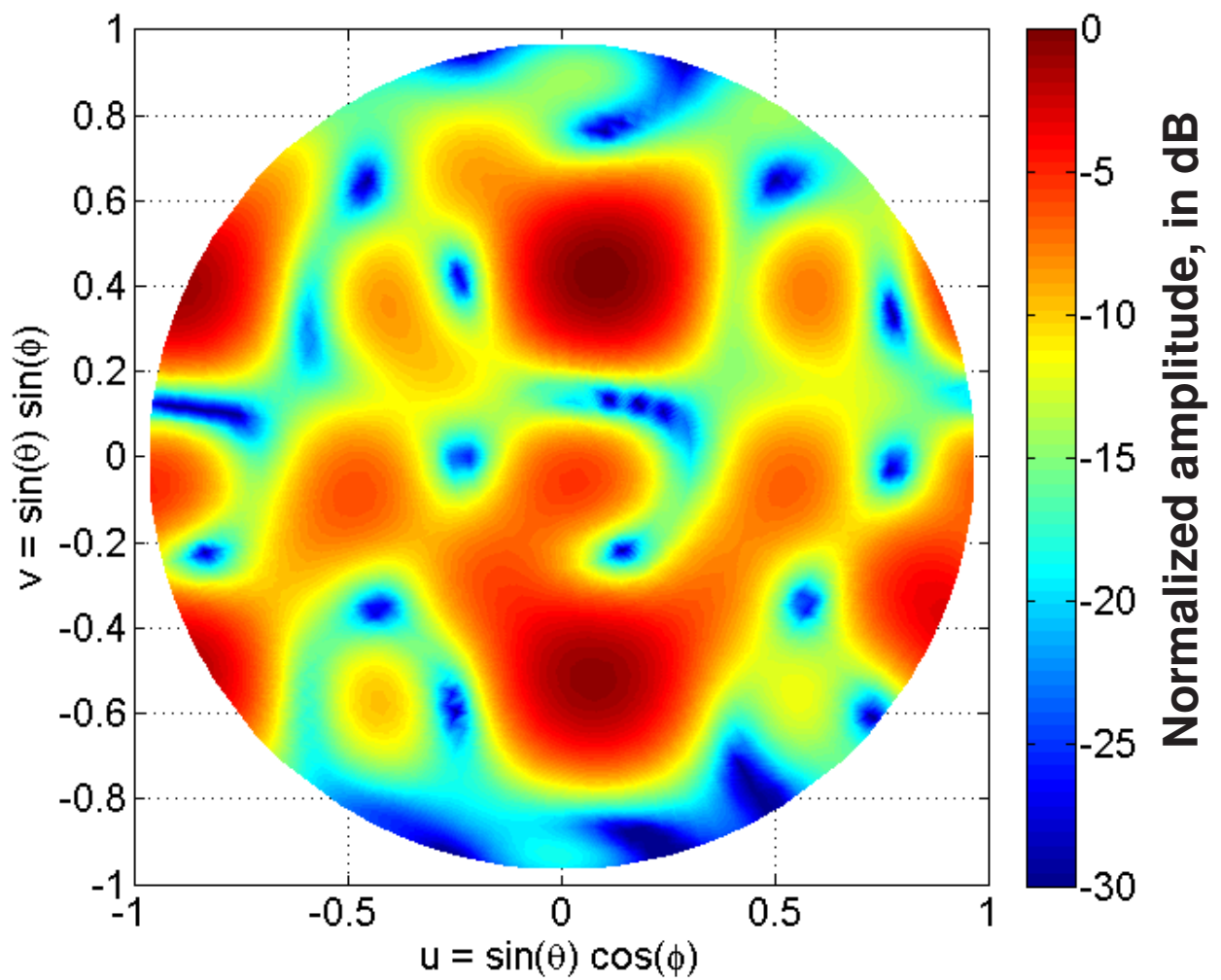
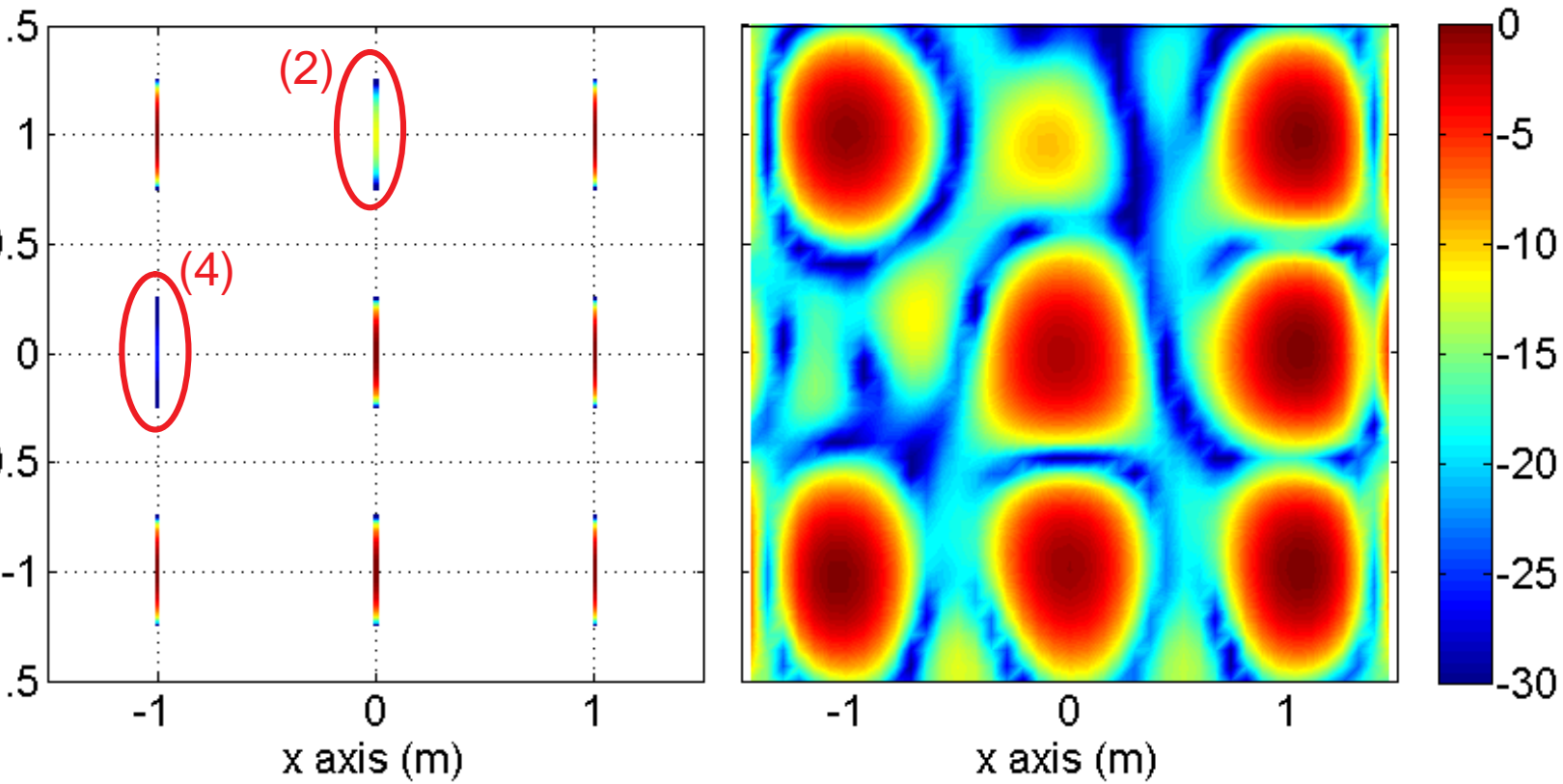


Figure 7. Array of dipoles. Top left: nominal excitations, in which dipoles 2 and 4 are distorted. Top right: reconstructed $M_{eq,x}$. Bottom: array of dipoles radiation pattern.

The application of Image Theory for this problem allows neglecting equivalent electric currents in the formulation, using just magnetic currents. The integral equation relating the spherical field tangential components E_θ , E_φ , with the magnetic currents components $M_{eq,u}$, $M_{eq,v}$ ($M_{eq,x}$, $M_{eq,y}$ for the particular case) can be expressed as a linear system of equations to be solved (8):

$$\begin{pmatrix} E_{rad}^\theta \\ E_{rad}^\varphi \end{pmatrix} = \begin{pmatrix} Z_{E_{rad}^\theta; M_{eq,x}} & Z_{E_{rad}^\theta; M_{eq,y}} \\ Z_{E_{rad}^\varphi; M_{eq,x}} & Z_{E_{rad}^\varphi; M_{eq,y}} \end{pmatrix} \begin{pmatrix} M_{eq,x} \\ M_{eq,y} \end{pmatrix} \quad (8)$$

The system has $N_e=441 \times 2$ equations, and $M_u=441 \times 2$ unknowns. As indicated before, one of the main drawbacks of inverse problems is the intrinsic ill-conditioning. The condition number of the Z-matrix in (8) has been calculated, and it is 3.9×10^{25} , or in other words, this is the relation between the highest and lowest singular values, which are plotted in Fig. 8.

The linear system of equations is solved using the Truncated SVD (T-SVD) (Álvarez et al., 2009b; Araque & Vecchi, 2010) and the Conjugate Gradient (CG) (Álvarez et al., 2009b; Álvarez et al., 2007), both of them providing the same results. In the case of the T-SVD, different thresholds are selected: the idea is that, by filtering the lowest singular values, the Z-matrix condition number decreases, then improving the matrix conditioning. With respect to the CG, the metric to evaluate the solution accuracy is based on the error between the simulated field and the field radiated by the reconstructed equivalent currents. The stopping criterion is set to $\Delta\varepsilon = \varepsilon(k-1) - \varepsilon(k) < 0.001$. For this problem, convergence was reached after 19 iterations ($\varepsilon = 0.019$), requiring just one minute of calculation in a conventional laptop.

To conclude this example, the reconstructed equivalent magnetic currents ($M_{eq,x}$) are plotted in Fig. 7. It is observed that the 9 elements (including the 2 distorted dipoles) are correctly identified, predicting also the amplitude on each.

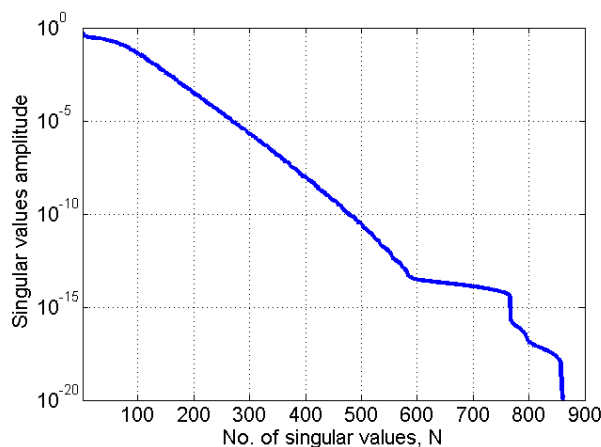


Figure 8. Singular values of the Z-matrix appearing in (8).

3.2. Phaseless measurements

The following application example is focused on antenna diagnostics and near-field to far-field transformation using phaseless information. The AUT is a logarithmic-periodic antenna working in the 400 MHz-3 GHz frequency band (Álvarez et al., 2010c). This antenna has been measured at the spherical range in anechoic chamber of the University of Oviedo, at two different distances: $R_1 = 3.20$ m, and $R_2 = 5.25$ m (see Fig. 9), and at the working frequency of $f = 1,030$ MHz. The field has been sampled on a full sphere: $\theta = [-180^\circ 180^\circ)$, $\Delta\theta = 4^\circ$, and $\varphi = [0^\circ 180^\circ]$, $\Delta\varphi = 4^\circ$, resulting in $N=4,140$ field samples on each acquisition sphere.

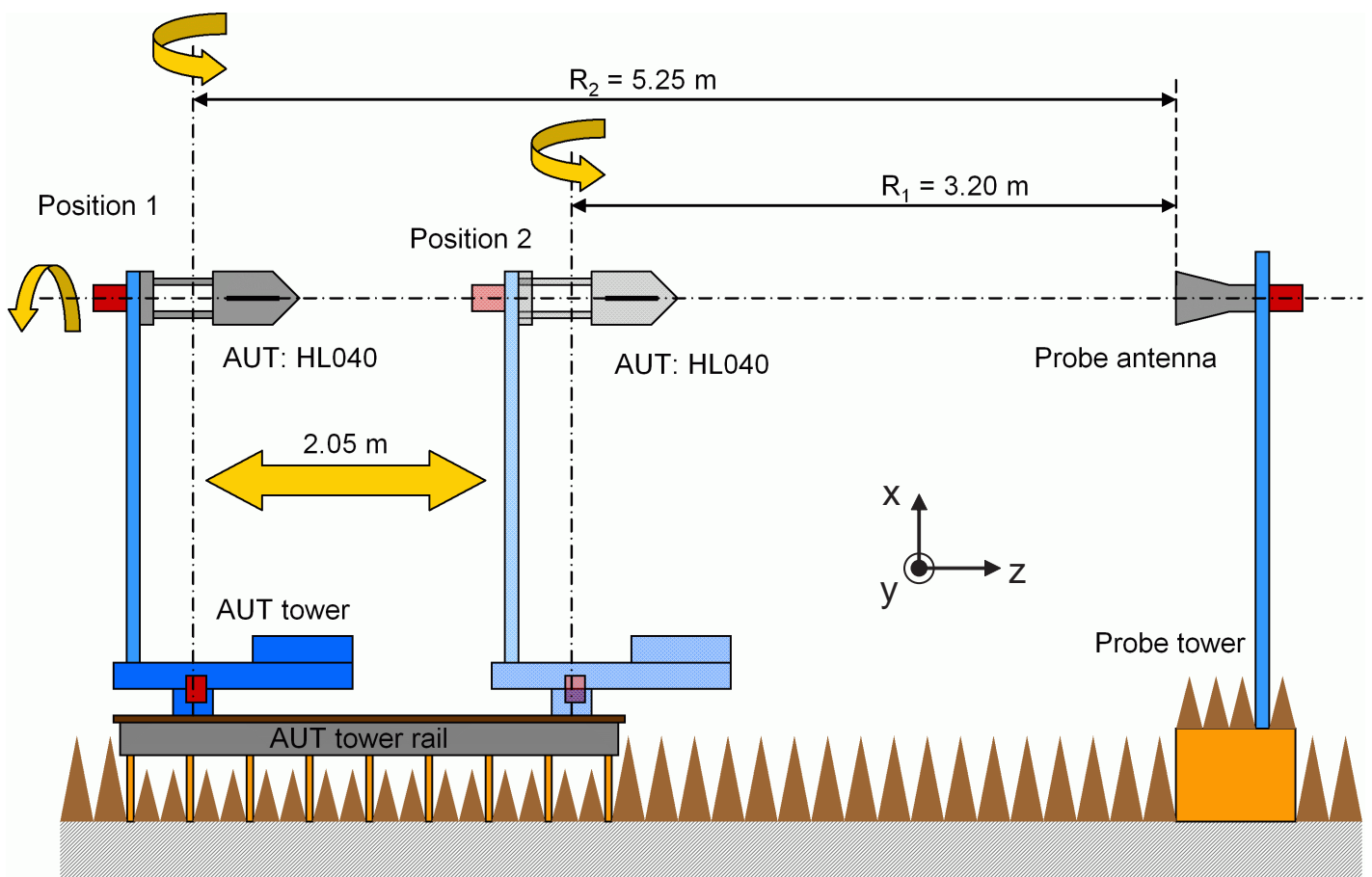


Figure 9. Antenna measurement at spherical range in anechoic chamber at two different distances.

The equivalent currents reconstruction domain is chosen to be a surface S' fitting the log-periodic antenna radome (see Fig. 10, (a),(b)). This surface is discretized into $M=3,298$ triangular facets. In consequence, taking into account the number of field samples on each sphere and the number of facets, the number of equations is $N_e=4,140 \times 2$ field components $\times 2$ measurement distances = 16,560, and the number of unknowns, $M_u = 3,298 \times 2$ type of currents $\times 2$ current components = 13,192.

Two different kinds of problems are now solved. First, the system of equations relating the

field samples (amplitude and phase) with the equivalent currents (9) is solved. The retrieved

currents are plotted in Fig. 10 (d),(f): it is observed that for the selected working frequency,

the resonant elements are placed in the middle of the log-periodic antenna (Álvarez et al.,

2010c; Álvarez et al., 2009b). As the elements are x-polarized (Fig. 10 (b)), only the $J_{eq,x}$ com-

ponent is plotted. Next, from the reconstructed equivalent currents, the field at any point of

the space can be calculated, and hence, far field radiation pattern of the log-periodic antenna

which is plotted in Fig. 11 (dark and gray solid lines).

$$\begin{pmatrix} E_{rad,R_1}^\theta \\ E_{rad,R_1}^\phi \\ E_{rad,R_2}^\theta \\ E_{rad,R_2}^\phi \end{pmatrix} = \begin{pmatrix} Z_{E_{rad,R_1}^\theta;J_{eq,u}} & Z_{E_{rad,R_1}^\theta;J_{eq,v}} & Z_{E_{rad,R_1}^\theta;M_{eq,u}} & Z_{E_{rad,R_1}^\theta;M_{eq,v}} \\ Z_{E_{rad,R_1}^\phi;J_{eq,u}} & Z_{E_{rad,R_1}^\phi;J_{eq,v}} & Z_{E_{rad,R_1}^\phi;M_{eq,u}} & Z_{E_{rad,R_1}^\phi;M_{eq,v}} \\ Z_{E_{rad,R_2}^\theta;J_{eq,u}} & Z_{E_{rad,R_2}^\theta;J_{eq,v}} & Z_{E_{rad,R_2}^\theta;M_{eq,u}} & Z_{E_{rad,R_2}^\theta;M_{eq,v}} \\ Z_{E_{rad,R_2}^\phi;J_{eq,u}} & Z_{E_{rad,R_2}^\phi;J_{eq,v}} & Z_{E_{rad,R_2}^\phi;M_{eq,u}} & Z_{E_{rad,R_2}^\phi;M_{eq,v}} \end{pmatrix} \begin{pmatrix} J_{eq,u} \\ J_{eq,v} \\ M_{eq,u} \\ M_{eq,v} \end{pmatrix} \quad (9)$$

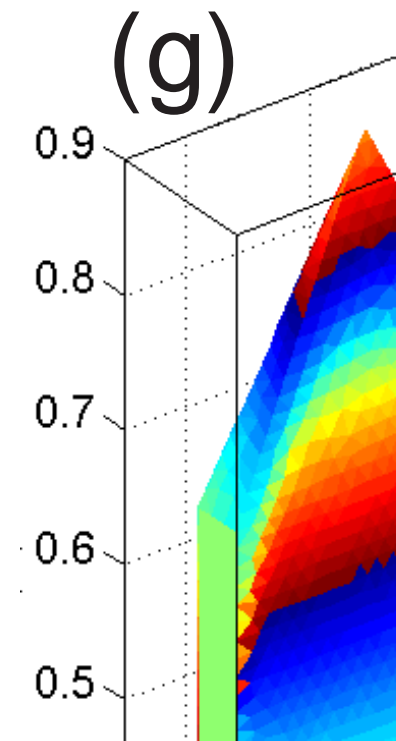
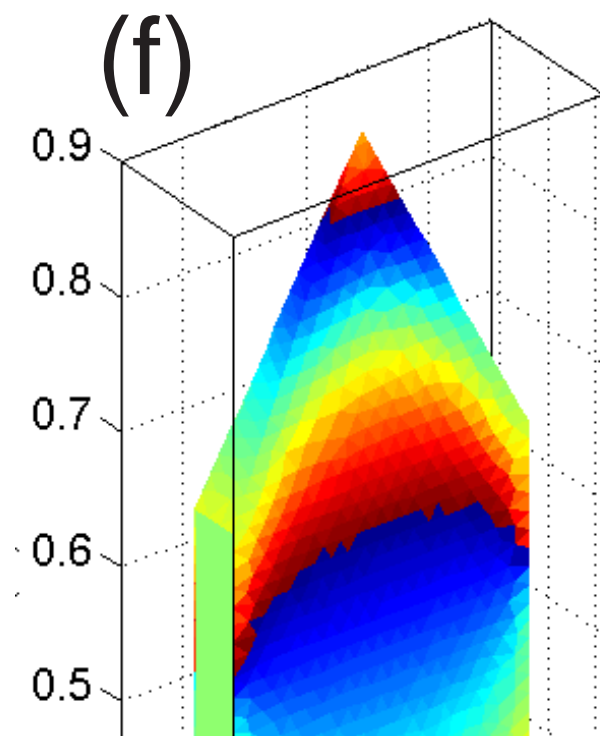
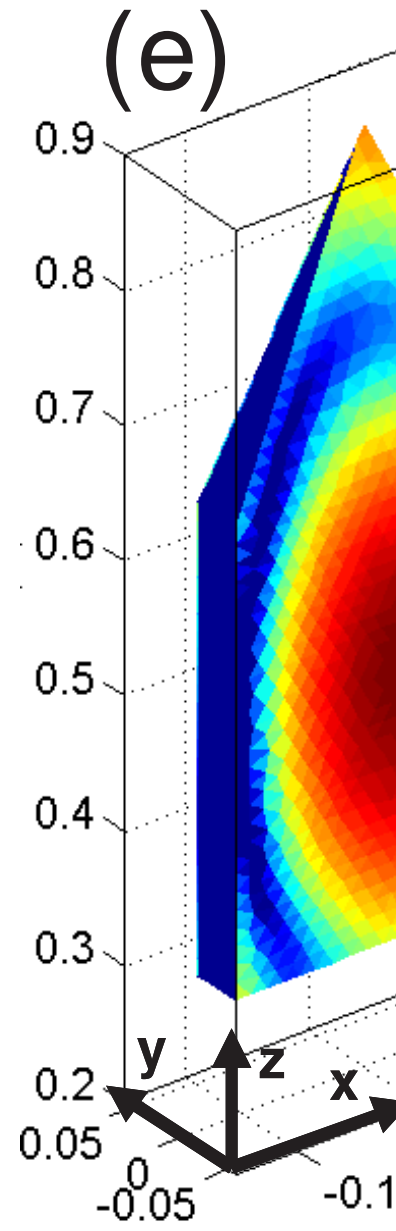
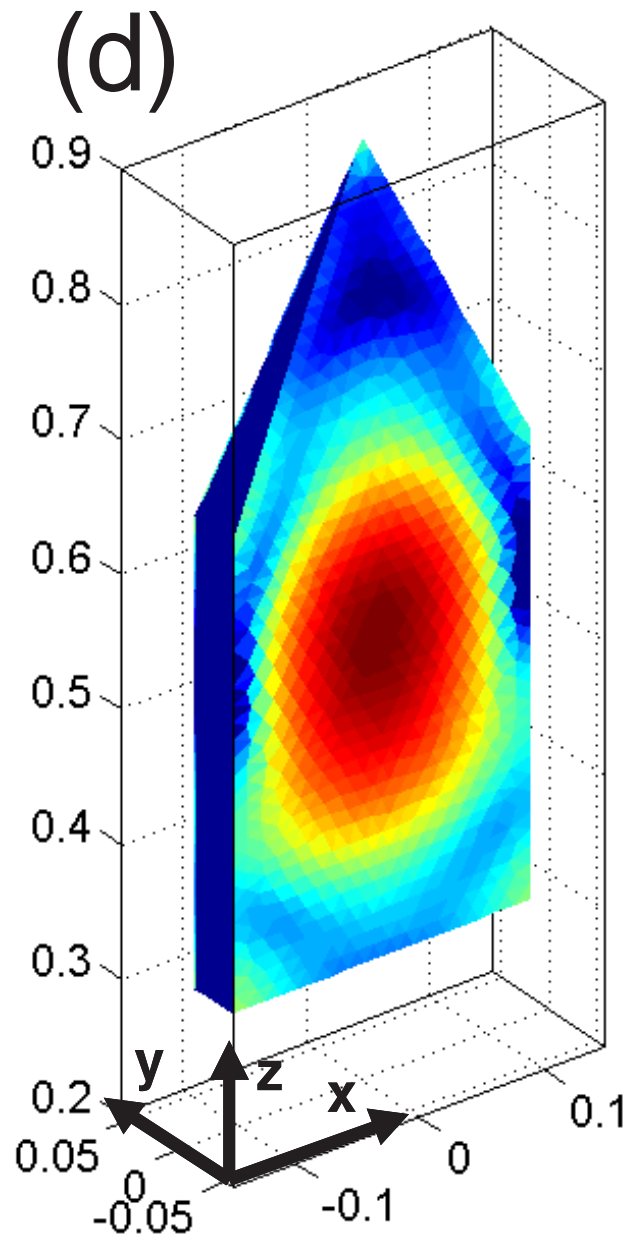
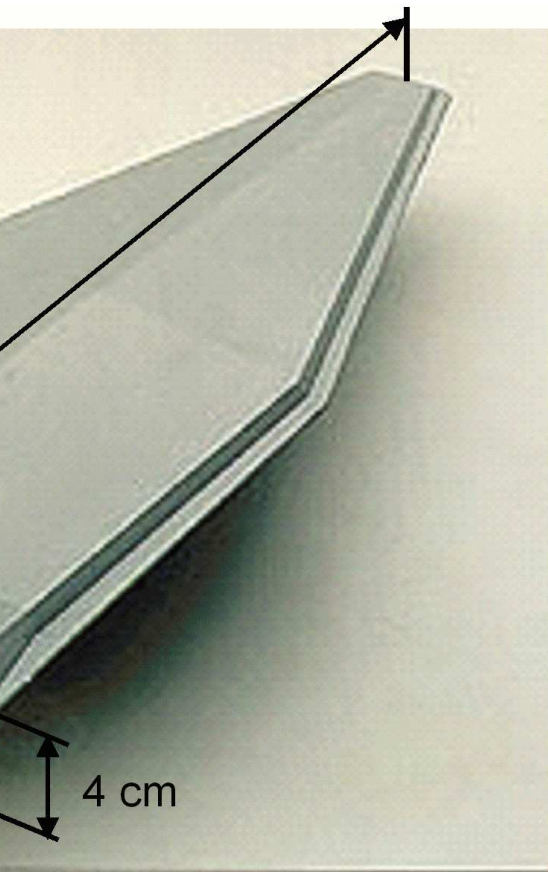


Figure 10. Photos: (a) log-periodic antenna array with radome. (b) Without radome. (c) Measurement at spherical range in anechoic chamber. Reconstructed equivalent currents, $J_{eq,x}$ component. (d),(f) using amplitude and phase information. (e),(g) using amplitude-only information.

The second problem to be solved neglects the phase information of the field samples. A non-linear system of equations, relating the amplitude of the field samples with the amplitude of the field radiated by the equivalent currents (10), has to be solved.

$$\begin{pmatrix} |E_{rad,R_1}^\theta| \\ |E_{rad,R_1}^\phi| \\ |E_{rad,R_2}^\theta| \\ |E_{rad,R_2}^\phi| \end{pmatrix} = \begin{pmatrix} Z_{E_{rad,R_1}^\theta; J_{eq,u}} & Z_{E_{rad,R_1}^\theta; J_{eq,v}} & Z_{E_{rad,R_1}^\theta; M_{eq,u}} & Z_{E_{rad,R_1}^\theta; M_{eq,v}} \\ Z_{E_{rad,R_1}^\phi; J_{eq,u}} & Z_{E_{rad,R_1}^\phi; J_{eq,v}} & Z_{E_{rad,R_1}^\phi; M_{eq,u}} & Z_{E_{rad,R_1}^\phi; M_{eq,v}} \\ Z_{E_{rad,R_2}^\theta; J_{eq,u}} & Z_{E_{rad,R_2}^\theta; J_{eq,v}} & Z_{E_{rad,R_2}^\theta; M_{eq,u}} & Z_{E_{rad,R_2}^\theta; M_{eq,v}} \\ Z_{E_{rad,R_2}^\phi; J_{eq,u}} & Z_{E_{rad,R_2}^\phi; J_{eq,v}} & Z_{E_{rad,R_2}^\phi; M_{eq,u}} & Z_{E_{rad,R_2}^\phi; M_{eq,v}} \end{pmatrix} \begin{pmatrix} J_{eq,u} \\ J_{eq,v} \\ M_{eq,u} \\ M_{eq,v} \end{pmatrix} \quad (10)$$

The problem of antenna diagnostics using phaseless field samples has been addressed by different approaches. For example (Yaccarino & Rahmat-Samii, 1999; Razavi & Rahmat-Samii, 2007) introduces a plane-to-plane iterative backpropagation method for phase retrieval, that can be used for both near-field to far-field transformation and antenna diagnostics applications. Phaseless SRM is described in (Las-Heras & Sarkar, 2002): in this case, an equivalent magnetic currents distribution is calculated by minimizing a cost function which relates the amplitude of the measured field and the contribution due to the equivalent currents, similarly to Eq. (10). However, these techniques are restricted to flat reconstruction surfaces S' , whereas the problem to be solved comprises a 3D reconstruction domains S' . Thus, in order to solve Eq. (10), the two-stage algorithm described in (Álvarez et al., 2010c; Álvarez et al., 2012b) is applied.

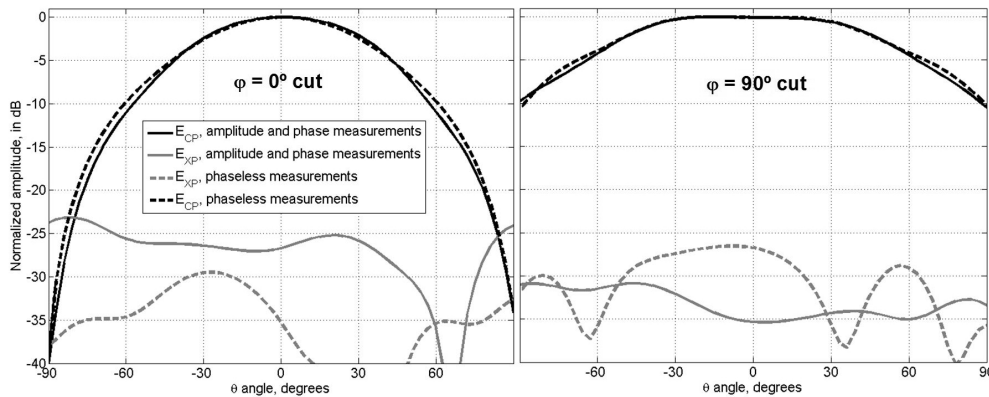


Figure 11. Log-periodic antenna far field pattern. Cuts $\phi = 0^\circ$ and $\phi = 90^\circ$. Comparison of the results when considering amplitude and phase field samples, and phaseless field samples.

The reconstructed equivalent currents from the phaseless field samples are plotted in Fig. 10 (e),(g), observing a good agreement with the ones retrieved from amplitude and phase information. It is important to remark that not only the amplitude, but also the phase of the equivalent currents (Fig. 10, (f),(g)) are in good agreement, proving the phaseless SRM for phase retrieval.

The latest step is the calculation of the log-periodic antenna radiation pattern from the reconstructed equivalent currents. The comparison between the radiation pattern from amplitude and phase information (Fig. 11, solid lines) and using phaseless information (Fig. 11, dashed lines) shows an acceptable agreement in the copolar component (black line). With regard to the crosspolar component, the amplitude levels are in the same order of magnitude (20-25 dB below the copolar component).

3.3. Geometry reconstruction applications

The latest example illustrates the SRM application for geometry reconstruction of metallic scatterers. A 2D problem is considered (Álvarez et al., 2010b) in which the object-under-test (depicted in Fig. 12, left plot) is supposed to have translation symmetry along one axis. The object is illuminated by 12 TM-polarized plane waves coming from 0° to 330° in 30° -steps. Four working frequencies are considered: 300, 450, 700 and 1,000 MHz. The scattered field is observed on a circumference of $R = 10$ m, sampled every 6° , which results in 60 field samples. Finally, noise is added according to a Signal-to-Noise (SNR) ratio of 30 dB.

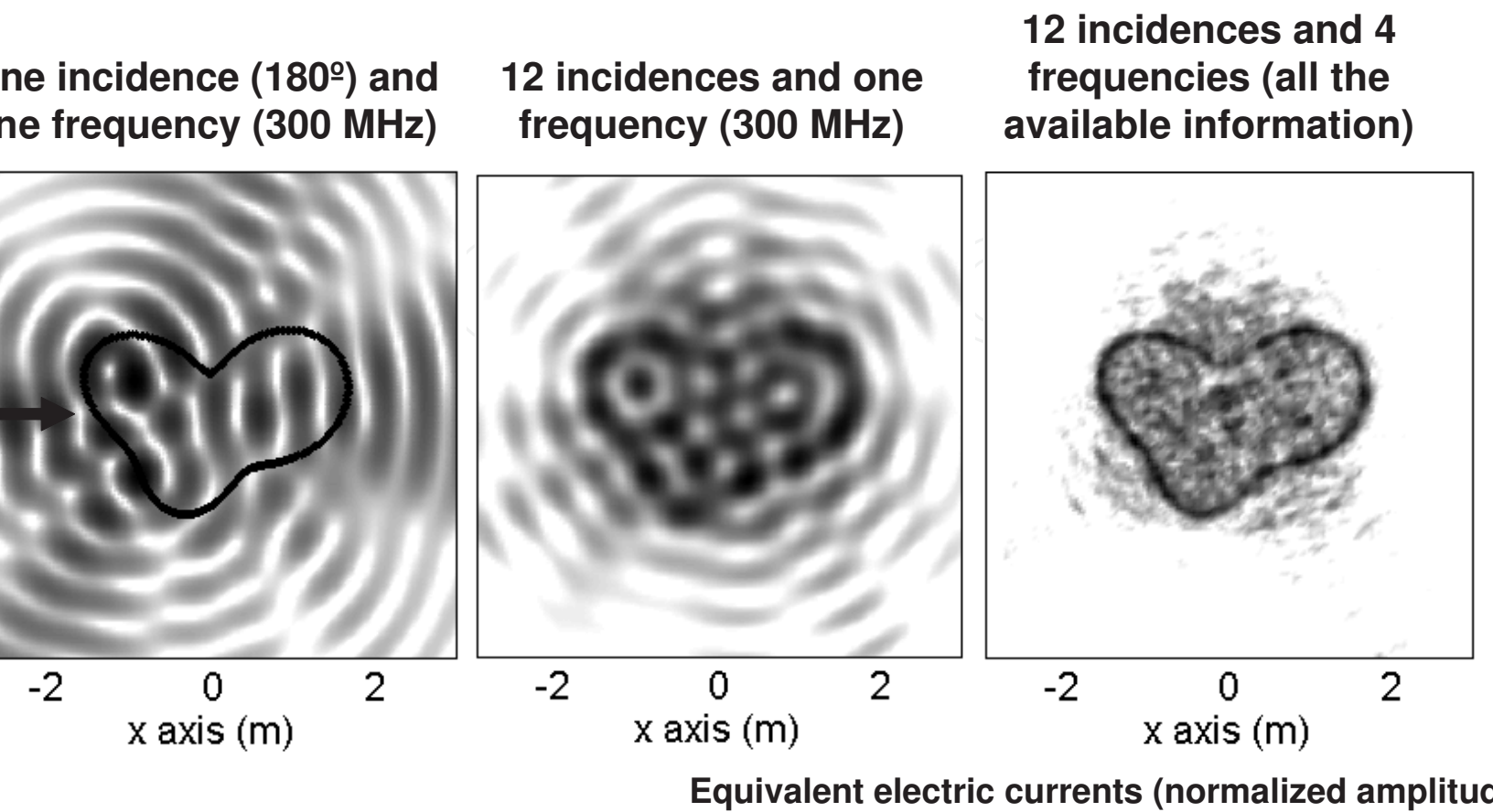


Figure 12. Geometry reconstruction application example. The solid line on the left plot indicates the true profile of the object-under-test.

The reconstruction domain V' is a square region of 6×6 m discretized into 121×121 square subdomains. Thus, for each incident wave and frequency, the system of equations to be solved has $N_e=60$ equations, and $M_u=14,641$ unknowns. The Conjugate Gradient algorithm is used, requiring about $K=9-11$ iterations to reach convergence ($\epsilon < 0.01$, $\Delta\epsilon < 0.001$).

First, the inverse problem for one frequency (300 MHz) and one incidence (180°) is solved. The reconstructed equivalent electric currents are plotted in Fig. 12 (left). The highest intensity of the reconstructed equivalent currents is located on the boundary of the object-under-test and, in particular, the part of the contour illuminated by the plane wave.

Combination of multiple incidences yields to a complete retrieval of the profile of the object-under-test. For example, the center plot of Fig. 12 represents the combination of the equivalent currents reconstructed for every incident plane wave at 300 MHz. The object-under-test profile can be now guessed. Higher resolution is provided by combining multifrequency information: the right plot of Fig. 12 clearly shows a well-defined profile.

4. Conclusion

The Sources Reconstruction Method for antenna diagnostics, near-field to far-field transformation, and geometry reconstruction applications has been described. The interest on this non-invasive technique is supported by several features which, in summary, are:

- i) Establishment of an accurate equivalent electromagnetic model of the AUT that can be used to evaluate the electromagnetic field at any point of the space.
- ii) The capability of handling arbitrary field acquisition and extreme near-field reconstruction domains, overcoming other diagnostics techniques limitation to canonical domains.
- iii) Reliability and accuracy as the method uses full-wave integral equation formulation.
- iv) The possibility of implementation on low cost GPU cards, enabling fast calculation even in conventional computers as those ones that can be found in antenna measurement facilities. Low memory footprint is also kept thanks to a developed memory saving technique (López et al., 2012).
- v) Extension to phaseless measurements, which is of special interest for sub-mm and THz systems in which phase measurements are especially complex and expensive.

Acknowledgements

This work has been supported by the European Union under COST Action IC1102 (VISTA); by the “Ministerio de Ciencia e Innovación” of Spain/FEDER under projects CONSOLIDER-INGENIO CSD2008-00068 (TERASENSE), TEC2011-24492/TEC (iSCAT), IPT-2011-0951-390000 (TECNIGRAF), and under PhD grant BES-2009-024060; and by the “Gobierno del Principado de Asturias” PCTI-FEDER under project PC10-06 (FLEXANT).

Author details

Yuri Álvarez*, Fernando Las-Heras and Cebrián García

*Address all correspondence to: yurilope@gmail.com

Área de Teoría de la Señal y Comunicaciones – Universidad de Oviedo, Spain

References

- [1] Álvarez, Y., Las-Heras, F., & Pino, M. R. (2007). Reconstruction of Equivalent Currents Distribution Over Arbitrary Three-Dimensional Surfaces Based on Integral Equation Algorithms. *IEEE Transactions on Antennas and Propagation*, 54, 3460-3468.
- [2] Álvarez, Y., Las-Heras, F., & Pino, M. R. (2008). On the Comparison between the Spherical Wave Expansion and the Sources Reconstruction Method. *IEEE Transactions on Antennas and Propagation*, 56(10), 3337-3341.
- [3] Alvarez, Y., Las-Heras, F., Pino, M. R., & López, J. (2008). Acceleration of the Sources Reconstruction Method via the Fast Multipole Method. *2008 IEEE International Symposium on Antennas and Propagation (APS'08)*, San Diego, CA (USA) 5-12 July 2008.
- [4] Alvarez, Y., Cappellin, C., Las-Heras, F., & Breinbjerg, O. (2008). On the comparison of the Spherical Wave Expansion-to-Plane Wave Expansion and the Sources Reconstruction Method for Antenna Diagnostics. *Progress In Electromagnetics Research*, PIER 87, 245-262.
- [5] Alvarez, Y., Las-Heras, F., & Pino, M. R. (2009). Application of the Adaptive Cross Approximation Algorithm to the Sources Reconstruction Method. *3rd European Conference on Antennas and Propagation (EUCAP'09)*, Berlin (Germany), 23-27 March 2009, 1-5.
- [6] Álvarez, Y., Las-Heras, F., Pino, M. R., & Sarkar, T. K. (2009). An Improved Super-Resolution Source Reconstruction Method. *IEEE Transactions on Instrumentation and Measurement*, 58(11), 3855-3866.
- [7] Álvarez, Y., Casas, B. A., García, C., & Las-Heras, F. (2010). The Volumetric Sources Reconstruction Method and its Applications to Geometry Reconstruction. *4th European Conference on Antennas and Propagation (EUCAP'10)*, Barcelona (Spain), 12-16 April 2010, 1-5.
- [8] Álvarez, Y., Casas, B. A., García, C., & Las-Heras, F. (2010). Geometry Reconstruction of Metallic Bodies Using the Sources Reconstruction Method. *IEEE Antennas and Wireless Propagation Letters*, 9, 1197-1200.
- [9] Álvarez, Y., Las-Heras, F., & Pino, M. R. (2010). The Sources Reconstruction Method for Amplitude-Only Field Measurements. *IEEE Transactions on Antennas and Propagation*, 58(8), 2776-2881.
- [10] Álvarez, Y., Martínez, J. A., Las-Heras, F., & Rappaport, C. (2011). An Inverse Fast Multipole Method for Imaging Applications. *IEEE Antennas and Wireless Propagation Letters*, 10, 1259-1262.
- [11] Álvarez, Y., Martínez, J. A., Las-Heras, F., & Rappaport, C. (2012). An inverse Fast Multipole Method for geometry reconstruction using scattered field information. *IEEE Transactions on Antennas and Propagation*, 60(7), 1-9, In press.

- [12] Álvarez, Y., Las-Heras, F., & Pino, M. R. (2012). Antenna Diagnostics Using Phaseless NF Information. *AUTOMATIKA Journal for Control, Measurement, Electronics, Computing and Communications*, 53(1), 49-55.
- [13] Araque, J., & Vecchi, G. (2009). Removal of unwanted structural interactions from antenna measurements. *Antennas and Propagation Society International Symposium, 2009, APSURSI'09*. Charleston, South Caroline, USA. June 2009.
- [14] Araque, J., & Vecchi, G. (2010). Field And Source Equivalence In Source Reconstruction On 3D Surfaces. *Progress In Electromagnetics Research, PIER* 103, 67-100.
- [15] Balanis, C. A. (1997). *Antenna Theory. Analysis and Design*, John Wiley & Sons.
- [16] Cano, F. J., Sierra-Castañer, M., Burgos, S., & Besada, J. L. (2010). Applications of sources reconstruction techniques: Theory and practical results. *Proceedings of the Fourth European Conference on Antennas and Propagation (EuCAP 2010)*, Barcelona, Spain. 12-16 April 2010, 1-5.
- [17] Caorsi, S., Gragnani, G. L., & Pastorino, M. (1990). Two-dimensional microwave imaging by a numerical inverse scattering solution. *IEEE Transactions on Microwave Theory and Techniques*, 38(8), 981-989.
- [18] Cappellin, C., Frandsen, A., & Breinbjerg, O. (2008). Application of the SWE-toPWE antenna diagnostics technique to an offset reflector antenna. *IEEE Antennas and Propagation Magazine*, 50(5), 204-213.
- [19] Cappellin, C., & Meincke, P. (2011). *Diatool* by TICRA. Brochure: <http://www.ticra.com/products/software/diatool-antenna-diagnostics>.
- [20] Coifman, R., Rokhlin, V., & Wandzuraz, S. (1993). The Fast Multipole Method for the Wave Equation: A Pedestrian Prescription. *IEEE Antennas and Propagation Magazine*, 35(3), 7-11.
- [21] Colton, D., Haddar, H., & Piana, M. (2003). The Linear Sampling Method in Inverse Electromagnetic Scattering Theory. *Inverse Problems*, 19, 105-137.
- [22] Eibert, T. F., & Schmidt, C. (2009). Multilevel fast multipole accelerated inverse equivalent current method employing Rao-Wilton-Glisson discretization of electric and magnetic surface currents. *IEEE Transactions on Antennas and Propagation*, 57(4), 1178-1185.
- [23] Engheta, N., Murphy, W. D., Rokhlin, V., & Vassiliou, M. S. (1992). The Fast Multipole Method (FMM) for Electromagnetic Scattering Problems. *IEEE Transactions on Antennas and Propagation*, 40(6), 634-641.
- [24] Farmahini, M. (2009). Fast and Accurate Cascaded Particle Swarm Optimization Method for solving 2-D Inverse Scattering Problems. *Journal of Applied Computational Electromagnetic Society, ACES*, 24(5), 1-4.
- [25] Foged, L. J., Scialacqua, L., Saccardi, F., Sabbadini, M., Araque, J. L., & Vecchi, G. (2011). Practical Application of the Equivalent Source Method as an Antenna Diag-

- nostics Tool. *2011 Antenna Measurement Techniques Conference (AMTA 2011)*, Denver, Colorado (USA). 17-20 October, 1-5.
- [26] Foged, L. J., Scialacqua, L., & Saccardi, . (2011). *Microwave Vision Group*, Brochure; http://www.microwavevision.com/sites/www.microwavevision.com/files/files/plaquette_insight_BD.pdf.
- [27] García, C., Álvarez, Y., Casas, B. A., & Las-Heras, F. (2011). Characterization of Antenna Interaction with Scatterers by means of Equivalent Currents. *Progress In Electromagnetics Research*, PIER 116, 185-202.
- [28] Gatti, M. S., & Rahmat-Samii, Y. (1988). FFT applications to plane-polar near-field antenna measurements. *IEEE Transactions on Antennas and Propagation*, 36, 781-791.
- [29] Habashy, T. M., Chow, E. Y., & Dudley, D. G. (1990). Profile inversion using the re-normalized source-type integral equation approach. *IEEE Transactions on Antennas and Propagation*, 38(5), 668-682.
- [30] Hajihashemi, M. R., & El-Shenawee, M. (2011). Inverse Scattering of Three-Dimensional PEC objects using the level-set method. *Progress In Electromagnetics Research PIER*, 116, 23-47.
- [31] Hansen, J. E. (1988). *Spherical Near-field Antenna Measurements*, IEE Electromagnetic Waves Series 26, London: Peter Peregrinus Ltd., 10.1049/PBEW026E.
- [32] Harrington, R. F. (2001). *Time-Harmonic Electromagnetic Fields*, John Wiley & Sons, 10.1109/9780470546710.
- [33] Hellicar, A. D., Hanham, S. M., Hislop, G., & Du, J. (2009). Terahertz Imaging with Antenna Coupled Detectors. *Proceedings on 3rd European Conference on Antennas and Propagation (EuCAP'09)*, Berlin, 23-27 March 2009, 1-5.
- [34] Hernando, M., Fernández, A., Arias, M., Rodríguez, M., Álvarez, Y., & Las-Heras, F. (2008). EMI Radiated Noise Measurements Using the Sources Reconstruction Technique. *IEEE Transactions on Industrial Electronics*, 55(9), 3258-3265.
- [35] Hislop, G., Li, L., & Hellicar, A. (2009). Phase Retrieval for Millimeter- and Submillimeter-Wave Imaging. *IEEE Transactions on Antennas and Propagation*, 57(1), 286-290.
- [36] Kaplan, L., Hanfling, J. D., & Borgiotti, G. V. (1979). The backward transform of the near field for reconstruction of aperture field. *IEEE Antennas and Propagation Society Symposium Digest*, 764-767.
- [37] Las-Heras, F. (2001). Using Equivalent Currents to Analyze Antennas in Complex Environments. *Microwave and Optical Technology Letters*, 31(1), 62-65.
- [38] Las-Heras, F., Pino, M. R., Loredó, S., Alvarez, Y., & Sarkar, T. K. (2006). Evaluating near field radiation patterns of commercial antennas. *IEEE Transactions on Antennas and Propagation*, 54, 2198-2207.

- [39] Las-Heras, F., Galocha, B., & Álvarez, Y. (2009). On The Sources Reconstruction Method Application For Array And Aperture Antennas Diagnostics. *Microwave and Optical Technology Letters*, 51(7), 1664-1668.
- [40] Las-Heras, F., & Sarkar, T. K. (2002). A direct optimization approach for source reconstruction and NF-FF transformation using amplitude-only data. *IEEE Transactions on Antennas and Propagation*, 50(4), 500-510.
- [41] Laviada, J., Álvarez, Y., & Las-Heras, F. (2010). Efficient determination of the near-field in the vicinity of an antenna for the determination of its safety perimeter. *Progress In Electromagnetics Research*, PIER 103, 371-391.
- [42] Lin, C. Y., & Kiang, Y. W. (1996). Inverse scattering for conductors by the equivalent source method. *IEEE Transactions on Antennas and Propagation*, 44(3), 310-316.
- [43] Livesay, D. E., & Chen, K.-M. (1974). Electromagnetic fields induced inside arbitrarily shaped biological bodies. *IEEE Transactions on Microwave Theory and Techniques*, 22(12), 1273-1280.
- [44] López, J. A., López, M., Álvarez, Y., García, C., Martínez, D., & Las-Heras, F. (2012). Fast Antenna Characterization Using The Sources Reconstruction Method on Graphics Processors. *Progress In Electromagnetics Research*, PIER 126, 185-201.
- [45] Lopez-Sanchez, J. M., & Fortuny-Guash, J. (2000). 3-D Radar Imaging Using Range Migration Techniques. *IEEE Transactions on Antennas and Propagation*, 48(5), 728-737.
- [46] Martinez, J. A., Gonzalez, B., Rappaport, C., Meana, J. G., & Pino, A. G. (2011). Reconstructing Distortions on Reflector Antennas With the Iterative-Field-Matrix Method Using Near-Field Observation Data. *IEEE Trans. on Antennas and Propagation*, 59(6), 2434-2437.
- [47] Mikki, S., & Kishk, A. (2007). Theory and Applications of Infinitesimal Dipole Models for Computational Electromagnetics. *IEEE Transactions on Antennas and Propagation*, 55(5), 1325-1337.
- [48] Persson, K., & Gustafsson, M. (2005). Reconstruction of equivalent currents using a near-field data transformation- with radome applications. *Progress In Electromagnetics Research*, PIER 54, 179-198.
- [49] Petre, P., & Sarkar, T. K. (1992). Planar near-field to far-field transformation using an equivalent magnetic current approach. *IEEE Transactions on Antennas and Propagation*, 40(11), 1348-1356.
- [50] Qin, Y. M., & Ciric, I. R. (1993). Inverse scattering solution with current modeling and Tikhonov regularization. *Proceedings on IEEE International Antennas and Propagation Symposium*, June 1993, 1, 492-495.
- [51] Rahmat-Samii, Y. (1984). Surface diagnosis of large reflector antennas using microwave holography metrology. *Radio Science*, 19, 1205-1217.

- [52] Rao, S. M., Wilton, D. R., & Glisson, A. W. (1982). Electromagnetic Scattering by Surfaces of Arbitrary Shape. *IEEE Transactions on Antennas and Propagation*, AP-30(3), 409-418, May 1982.
- [53] Razavi, S. F., & Rahmat-Samii, Y. (2007). A new look at phaseless planar near-field measurements: limitations, simulations, measurements, and a hybrid solutions. *IEEE Antennas and Propagation Magazine*, 49(2), 170-178.
- [54] Sarkar, T. K., & Arvas, E. (1981). On the class of finite step iterative methods (Conjugate Directions) for the solution of an operator equation arising in electromagnetics. *IEEE Transactions on Antennas and Propagation*, 29, 370-373.
- [55] Sarkar, T. K., Weiner, D., & Jain, K. V. (1981). Some Mathematical Considerations in Dealing with the Inverse Problem. *IEEE Transactions on Antennas and Propagation*, AP-29(2), March 1981.
- [56] Sarkar, T. K., & Taaghoul, A. (1999). Near-field to near/far-field transformation for arbitrary near-field geometry utilizing an equivalent current and MoM. *IEEE Transactions on Antennas and Propagation*, 47(3), 566-573.
- [57] Sijher, T. S., & Kishk, A. (2005). Antenna modeling by infinitesimal dipoles using genetic algorithms. *Progress In Electromagnetics Research*, PIER 52, 225-254.
- [58] Stratton, J. (1941). *Electromagnetic theory*. McGraw-Hill, New York.
- [59] Van den Berg, P. M., & Kleinman, R. E. (1997). A contrast source inversion method. *Inverse Problems*, 13, 1607-1620.
- [60] Wang, H.-C., & Hwang, K. (1995). Multicoloring of grid-structured PDE solvers for parallel execution on shared-memory multiprocessors. *IEEE Transactions on Parallel and Distributed Systems*, 6(11), 1195-1025.
- [61] Yaccarino, R. G., & Rahmat-Samii, Y. (1999). Phaseless bi-polar planar nearfield measurements and diagnostics of array antennas. *IEEE Transactions on Antennas and Propagation*, 47(3), 574-583.
- [62] Yaccarino, R. G., Rahmat-Samii, Y., & Williams, L. I. (1994). The bi-polar planar near-field measurement technique, part II: near-field to far-field transformation and holographic imaging methods. *IEEE Transactions on Antennas and Propagation*, 42, 196-204.
- [63] Yaghjian, A. D. (1986). An overview of near-field antenna measurements. *IEEE Transactions on Antennas and Propagation*, 34(1), 30-45.
- [64] Zhao, K., Vouvakis, M. N., & Lee, J.-F. (2005). The Adaptive Cross Approximation Algorithm for Accelerated Method of Moments Computations of EMC Problems. *IEEE Transactions on Electromagnetic Compatibility*, 47(4), 763-773.